Homogeneous, Micron-Scale High-Energy-Density Matter Generated by Relativistic Laser-Solid Interactions

N. F. Beier, H. Allison, P. Efthimion, K. A. Flippo, L. Gao, S. B. Hansen, K. Hill, R. Hollinger, M. Logantha, Y. Musthafa, R. Nedbailo, V. Senthilkumaran, R. Shepherd, V. N. Shlyaptsev, H. Song, S. Wang, F. Dollar, J. J. Rocca, and A. E. Hussein

Phys. Rev. Lett. **129**, 135001 — Published 21 September 2022

DOI: 10.1103/PhysRevLett.129.135001

Homogeneous, Micron-scale High Energy Density Matter Generated by Relativistic Laser-solid Interactions

N. F. Beier,[1,2] H. Allison,[2] P. Efthimion,[3] K. A. Flippo,[4] L. Gao,[3] S. B. Hansen,[5] K. Hill,[3] R. Hollinger,[6] M. Logantha,[2] Y. Musthafa,[2] R. Nedbailo,[6] V. Senthilkumaran,[1] R. Shepherd,[7] V. N. Shlyaptsev,[6] H. Song,[6] S. Wang,[6] F. Dollar,[2] J. J. Rocca,[6,8] and A. E. Hussein[1]

[1]*Department of Electrical and Computer Engineering, University of Alberta, Edmonton, AB T6G 2R3 Canada*
[2]*STROBE, NSF Science & Technology Center, University of California, Irvine, CA 92617 USA*
[3]*Princeton Plasma Physics Laboratory, Princeton, NJ 08536 USA*
[4]*Los Alamos National Laboratory, PO Box 1163, Los Alamos, NM, 87545 USA*
[5]*Sandia National Laboratories, Albuquerque, NM, 87185 USA*
[6]*Department of Electrical and Computer Engineering, Colorado State University, Fort Collins, CO 80521 USA*
[7]*Lawrence Livermore National Laboratory, Livermore, CA 94550 USA*
[8]*Department of Physics, Colorado State University, Fort Collins, CO 80521 USA*
(*nbeier@ualberta.ca)
(Dated: August 29, 2022)

Short-pulse, laser-solid interactions provide a unique platform for studying complex high-energy-density matter. We present the first demonstration of solid density, micron-scale keV plasmas uniformly heated by a high-contrast, 400 nm wavelength laser at intensities up to 2×10^{21} W/cm^2. High-resolution spectral analysis of X-ray emission reveals uniform heating up to 3.0 keV over 1 μm depths. Particle-in-cell simulations indicate the production of a uniformly heated keV plasma to depths of 2 μm. The significant bulk heating and presence of highly-ionized ions deep within the target are attributed to the few MeV hot electrons that become trapped and undergo refluxing within the target sheath fields. These conditions enabled the differentiation of atomic physics models of ionization potential depression in high energy density environments.

High-energy-density (HED) matter exists in extreme states of temperature and density characterized by energy densities exceeding 10^{11} J/m^3 and pressures exceeding 100 GPa [1]. Elucidating the temperature, pressure, and density in these HED environments is critical for understanding the physics of stellar interiors [2–5] and the achievement of inertial confinement fusion [6–8]. However, an accurate description of HED conditions remains an experimental and theoretical challenge due to the complex laser-plasma dynamics, heating mechanisms, and rapidly evolving plasma conditions.

The development of experimental platforms to generate well-characterized HED plasmas can provide a novel means to diagnose fundamental properties such as opacity and equations of state, needed to benchmark atomic physics models and simulations tools. In particular, the generation of homogeneous HED plasmas can minimize uncertainties in temperature and density profiles [9–16]. One common method to produce homogeneous HED conditions is the use of thin (10s - 100s nm) buried tracer layers to mitigate longitudinal gradients [9, 11, 17–19], however layered targets introduce new complications due to fields at material interfaces [20–22]. The generation of homogeneous, long length-scale, solid-density plasmas using mid-scale, short-pulse ($\tau < 100$ fs) ultra-intense laser facilities provides novel and accessible platforms for detailed experimental studies of HED plasmas.

During relativistic laser-solid interactions, ($I\lambda^2 \gtrsim 10^{18}$ Wcm^{-2}μm^2), electrons accelerated by the laser field to relativistic energies can transport energy from the laser focal area to the bulk material. These hot electrons are the dominant heating mechanism in solid targets [23–27]. Provided that these short-pulse lasers are of sufficiently high contrast (typically $\gtrsim 10^8$ intensity contrast), the laser will interact with a solid density target before significant hydrodynamic expansion can occur. Studies using high-contrast Ti:Sapphire laser systems in the second-harmonic (400 nm wavelength) focused to intensities $I \sim 10^{19}$ W/cm^2 have shown that the supra-thermal (∼0.4 MeV) electrons can heat near-solid density plasmas to approximately 100 eV over 5 μm lengths [28], or to >1 keV temperatures over 150 nm lengths [29]. At higher intensities, ($I > 10^{21}$ W/cm^2) and contrast ratios ($>10^{12}$ intensity contrast) highly-ionized, near-solid density plasmas over several microns have been created by irradiating gold nanowire targets [30]. However, to the best of our knowledge, a uniformly heated, multi-keV, solid density plasma with micron scale lengths has not yet been demonstrated.

K-shell X-ray emission spectroscopy is a widely used diagnostic of the temperature, density, and hot electron dynamics of laser-produced plasmas [26, 29, 31–37]. During the propagation of hot electrons through cold, neutral material, cold inner-shell emission, e.g. Kα and Kβ, is produced via collisional-ionization of inner-shell electrons before the transition of an L or M-shell electron to fill the vacancy [33, 38, 39]. Conversely, the appearance of thermal ionic emission lines, e.g. Heα and Lyα, are due to electronic transitions from highly-ionized atoms, namely from helium-like and hydrogen-like ions for Heα and Lyα, respectively. These highly-ionized atoms are typically generated within the thermal plasma in the central hot-spot of the laser focus [33, 35].

In this Letter, we demonstrate the generation of uniformly heated, multi-keV, solid-density plasmas through laser-solid interactions using a high-contrast, 400 nm laser at intensities up to $I = 2\times10^{21}$ W/cm^2. High-resolution X-ray spectroscopy of K-shell emission from atoms ionized up to H-like copper (Cu) indicate that solid-density plasmas were volumetrically heated to multi-keV temperatures over the first 2 μm. The homogeneous heating by the 400 nm wavelength laser is

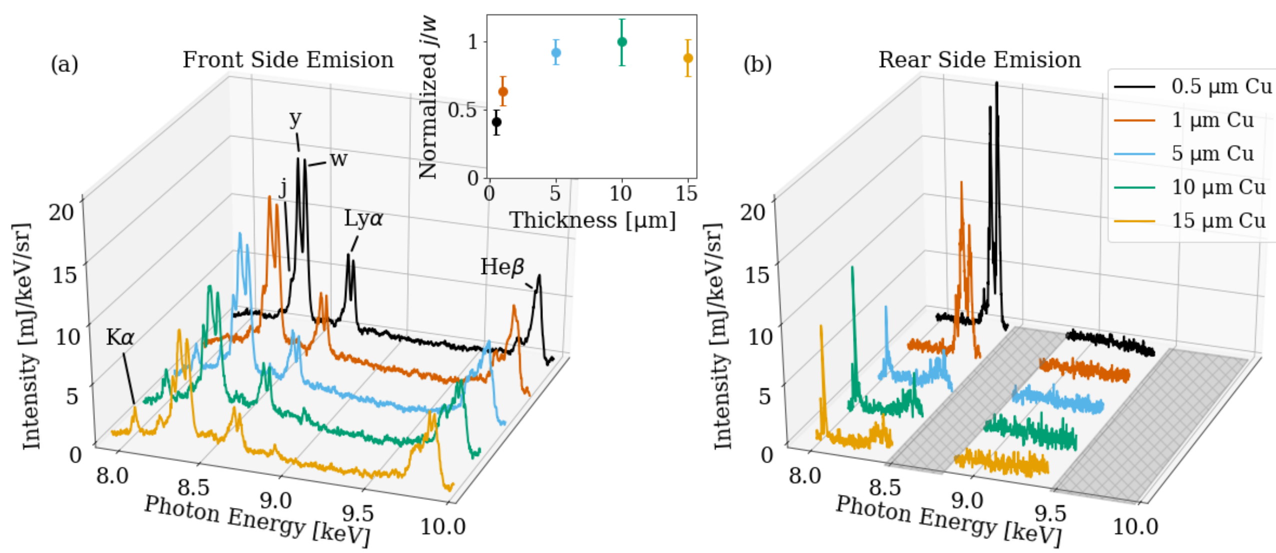

FIG. 1. Front-side (a) and rear-side (b) Cu foil emission irradiated by the 400 nm laser at 2×10^{21} W/cm^2. Lines represent three shot averages. Inset of (a): Calculated normalized ratio of the j Li-like satellite to w Heα resonance. Gray cross-hatched bars in (b) denote regions outside the dispersion range of the high-resolution spectrometer.

attributed to the generation of few MeV electrons with favorable conditions to become trapped and undergo refluxing in within few-micron targets, as opposed to higher energy electrons generated at 800 nm that experience less trapping, resulting in colder material. These results demonstrate an approach for generating homogeneous, micron-scale HED matter using simple, single-material flat foils that can be used as a platform for validation of atomic physics models.

Experiments were conducted by irradiating Cu foil targets with the 400 nm and 800 nm wavelength modes of the ALEPH laser [40]. The ALEPH 400 nm mode delivered up to 6.6 ± 0.2 J pulses of 45 fs Full-Width-at-Half-Maximum (FWHM) duration in a focal spot of 1.5 ± 0.2 μm FWHM to obtain intensities of $2.9\pm0.8\times10^{21}$ W/cm^2 with an intensity contrast of 10^{16} at times > 5 ps preceding the laser pulse. Cu foils of 0.5 - 15 μm thickness were irradiated at normal incidence. The 800 nm mode delivered 12.4 ± 0.4 J pulses with 30 fs FWHM with a focal spot size of 2.4 ± 0.2 μm FWHM, producing intensities of $3.2\pm0.5\times10^{21}$ with an intensity contrast of 10^8 within 5 ps. Cu foils of 1 - 15 μm thickness were irradiated at a 10° angle-of-incidence. Copper K-shell spectra were measured using two spectrometers: (1) a moderate-resolution ($E/\Delta E\sim1000$) von Hamos mica crystal spectrometer (VHS) and (2) a high-resolution ($E/\Delta E>7500$) spectrometer (HRS) consisting of two spherical germanium crystals. Front-side emission was captured using the VHS and rear-side emission using the HRS, with viewing angles of 0° and 45° from target normal, respectively. A quartz-2131 spherical crystal imager was fielded to obtain rear-side Kα emission. Additional experimental details are provided in the Supplemental Material [41].

Collisional-radiative modeling using the SCRAM code [42] was used to determine plasma heating profiles through fitting of synthetic spectra to experimental measurements. A series of SCRAM calculations (see Supplemental Material [41]) were performed to model the X-ray emission of solid density Cu layers of incremental thickness, $dx=0.1$ μm, with electron and ion temperatures $T_e=T_i=T$ ranging from 0.1 - 4.0 keV. Layers with various temperature profiles were stacked to simulate foils of different thicknesses. Global optical depth effects were incorporated in the fitting procedure, which transports the emission through each layer along the line of sight to the spectrometers.

Details of the heating process were further studied using three-dimensional (3D) PIC simulations performed in VLPL [43]. The simulations were initialized with singly ionized species of solid-density 12 μm × 12 μm Cu targets of 1, 2, and 5 μm thicknesses. A 7 J, 45 fs, 400 nm pulse with a spot size of 1.5 μm FWHM, producing a peak laser intensity of 3×10^{21} W/cm^2, was simulated, where $t=0$ fs corresponds to the peak of the pulse arriving at the surface of the target. Due to the high-contrast of the 400 nm ALEPH laser, no pre-plasma was simulated. Ionization effects due to optical field ionization (OFI) and electron-ion collisions were included.

X-ray spectra from Cu foil targets are plotted in Fig. 1. Fig. 1 (a) shows the front-side emission from Cu foils in which ionic line emission, i.e. Heα (8.35 keV), Lyα (8.69 keV) and Heβ (9.87 keV), was observed for all thicknesses, with an increase in Li-like Cu for increasing target thicknesses. Cold Kα (8.04 keV) and Kβ (8.91 keV) front-side emission were only observed for targets thicker than 5 μm. In rear-side emission, He-like Cu was observed for 0.5 and 1 μm thick foils (Fig. 1 (b)), while only a strong Kα doublet was observed for thicker targets. When irradiated at lower laser intensities ($\sim10^{20}$ W/cm^2), the only observed front-side and rear-side emission lines from all target thicknesses were Kα and Kβ.

Three emission lines have been marked in Fig. 1 (a) using Gabriel's notation [44]. These are the 1s2p $^1P_1\rightarrow1s^2\ ^1S_0$ Heα resonance transition (w), the 1s2p $^3P_1\rightarrow1s^2\ ^1S_0$ intercombination (y), and the Li-like dielectronic satellite (j). The ratio of the front-side j/w emission describes the relative populations of Li-like and He-like Cu [45, 46] and is plotted for front-side emission as a function of target thickness in the inset of Fig. 1 (a). The normalized ratio of j/w was found to increase for targets of 0.5, 1 and 5 μm thickness before plateauing at 10 and 15 μm , indicating that the X-ray-weighted electron temperature T_e decreases as the target thickness increases.

The presence of thermal Heα and Lyα emission in front-side and rear-side spectra from ≤ 1 μm thick foils in Fig. 1 (a) indicates that foils were volumetrically heated to keV temperatures by the 400 nm laser pulses. However, absence of Heα in rear-side measurements of targets with thicknesses ≥ 5 μm (Fig. 1 (b)) suggests significant absorption from a population of He-like ion species in a dense, hot plasma, but insufficient heating to generate strong emission lines from these ions [47]. Given the similar charge distribution of the emitting plasma inferred from the front-side emission of varying thickness, the strong absorption of rear-side He-like emission observed for targets > 1 μm suggests that a region of hot, opaque plasma exists over the first 1-5 μm of the plasma. Furthermore, the front-side and rear-side Kα emission from ≥ 5 μm targets is produced in regions of cold plasma, which do not reach highly-ionized charge states. These observations are consistent with the trends in plasma line emission as a function of target thickness in the insert of Fig. 1 (a).

Comparisons between SCRAM modeling and experimental data enabled investigation of temperature profiles in the resultant plasma [41]. Fig. 2 (a) and (b) show front-side and rear-side emission of 0.5 μm Cu foils, respectively, with a best fit using a constant temperature of $T = 3.5$ keV. Fig. 2 (c) and (d) show front-side and rear-side emission of 1 μm Cu foils, respectively, with a best fit constant temperature of $T = 3$ keV. However, constant temperature profiles did not reproduce both the front-side and rear-side spectra for targets ≥ 5 μm; temperature gradients were required to fit experimental measurements. Fig. 2 (e) and (f) show front-side and rear-side emission of 5 μm foils, respectively, with best-fit temperature profiles as the insets in Fig. 2 (e). The observed decrease in plasma temperature and appearance of temperature gradients agrees well with the measured increase in front-side j/w ratio (Inset Fig. 1 (a)), which indicates an increase in population of Li-like Cu ions.

The electron temperature and density profiles produced by the 400 nm interaction were further analyzed from 3D PIC simulations. The average electron temperature and density as a function of depth along the laser-axis at $t = 429$ fs in the simulation are plotted in Fig. 3 (a) and (b), respectively. The electron temperatures were calculated using the slope-temperature of a Maxwellian fit to the electron energy distribution. Cu foils of 1 μm and 2 μm thickness were found to have uniform temperature and density profiles of along the laser axis of $T_e \simeq 5.5$ keV and $n_e \simeq 1.54 \times 10^{24}$ cm^{-3}, and $T_e \simeq 3.5$ keV and $n_e \simeq 1.47 \times 10^{24}$ cm^{-3}, respectively. Conversely, 5 μm targets exhibited average electron temperature and density gradients, varying from $T_e \simeq 2.5$ keV and $n_e \simeq 1.41 \times 10^{24}$ cm^{-3} near the target surface to $T_e \simeq 0.25$ keV and $n_e \simeq 0.94 \times 10^{24}$ cm^{-3} at a depth of 5 μm. The results from PIC simulations indicate that homogeneous, multi-keV

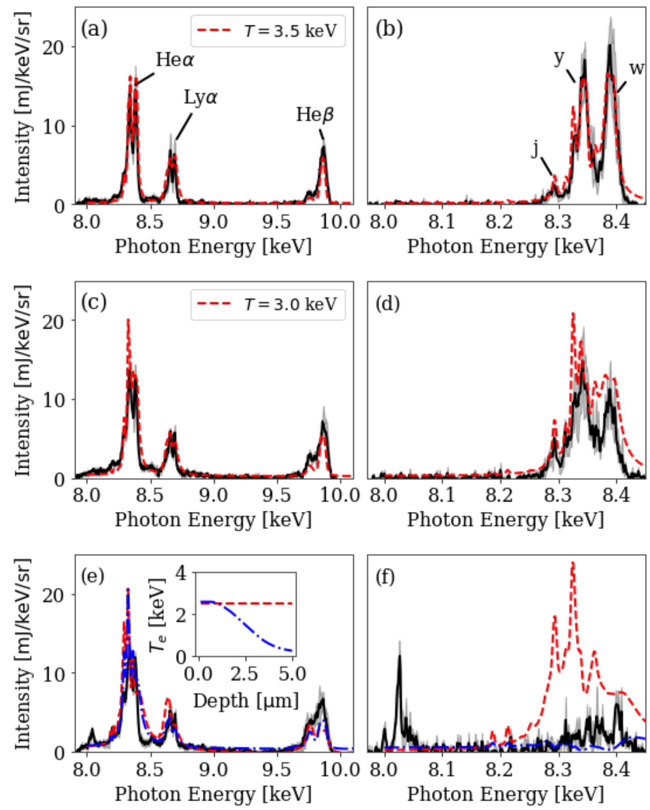

FIG. 2. Experimental Cu K-shell emission (black with shaded error bars) compared to SCRAM simulations with constant (dashed red) and variable (dash-dotted blue) temperature profiles. Front-side (a) and rear-side (b) spectra of 0.5 μm foil with constant temperature of 3.5 keV. Front-side (c) and rear-side (d) spectra of 1 μm foil with constant temperature of 3 keV. Front-side (e) and rear-side (f) spectra of 5 μm foil with constant and variable profiles (inset).

plasma are heated over micron-scale depths, in good agreement with experimental and SCRAM results. The agreement between the SCRAM analysis and PIC simulations indicate that the homogeneous plasmas have electron densities greater than 60 % of solid-density ($n_e = 2.3 \times 10^{24}$ cm^{-3} for He-like Cu) while reaching temperatures $T_e > 3$ keV.

Measurements of rear-side Kα emission were used to infer the area of hot electron propagation and approximate the bulk plasma heating volume [41]. Assuming that the average FWHM area of 69 ± 1 μm^2 of Kα emission corresponds to the region of multi-keV heating, the volume of uniform plasma generated by the 0.5 μm and 1 μm targets are 35 ± 1 μm^3 and 69 ± 1 μm^3, respectively. For solid density plasmas and a Maxwellian electron distribution, the total energy within these bulk plasma electrons is 68 mJ and 115 mJ, respectively, with conversion efficiency from laser to bulk plasma electrons on the order of 1 - 3%, consistent with 3% estimated from PIC simulations. From the Kα conversion efficiency, the absorption fraction of laser-to-hot-electrons is estimated to be 5-10% [48], consistent with other results from high-intensity laser interactions at normal incidence [49].

The generation of He-like and H-like Cu ions through OFI

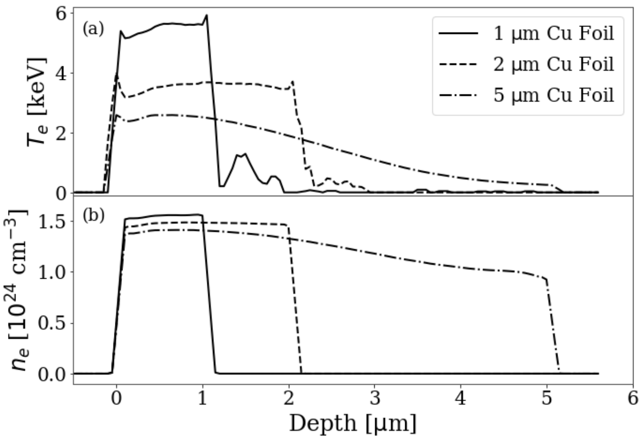

FIG. 3. 3D PIC results of 400 nm interaction. Electron temperature (a) and density (b) as a function of depth for 1 μm (solid), 2 μm (dashed), and 5 μm (dash-dotted) targets.

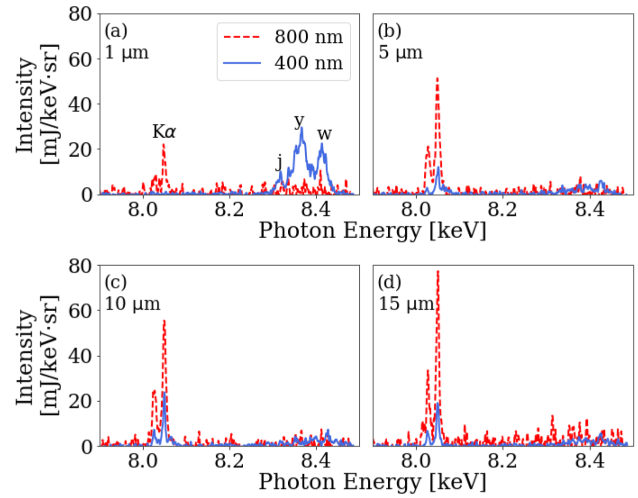

FIG. 4. Rear-side spectra of 1 μm (a), 5 μm (b), 10 μm (c), and 15 μm (d) thick Cu foil targets from 800 nm (dashed red) and 400 nm (solid blue) interactions.

require appearance intensities of 2×10^{20} W/cm^2 and 7×10^{21} W/cm^2, respectively. However, OFI only occurs within the laser skin depth. At relativistic intensities, the laser penetration depth is determined by the relativistic critical density $n_{\rm crit,rel} = \gamma n_{\rm crit}$, where γ is the relativistic Lorentz factor and $n_{\rm crit} = m_e\omega_0^2\varepsilon_0 e^{-2}$ is the non-relativistic critical density. At 400 nm, a relativistic factor of $\gamma \approx 11$ leads to a relativistic critical density of $n_{\rm crit,rel} \approx 10^{23}$ cm^{-3}, which remains an order of magnitude below the electron densities produced in solid-density He-like Cu ($n_{\rm e} = 2.3\times10^{24}$ cm^{-3}). The ultra-high contrast of the ALEPH 400 nm mode minimizes foil expansion prior to the arrival of the main pulse, reducing the propagation of the laser field to deep within the solid-density target [16, 30]. However, the observation of Heα emission from the rear-side of 0.5 μm and 1 μm targets (Fig. 1 (b)) requires the creation of He-like ions near the rear-surface at depths greater than those achievable by OFI under these circumstances. Therefore, the bulk heating must be driven by a population of energetic electrons generated within the laser skin depth at the relativistic critical density surface, which can propagate deep into the solid-density target.

Comparison of X-ray emission spectra obtained using the 400 nm and 800 nm modes of the ALEPH laser give insight into energetic electron dynamics and wavelength-dependent heating mechanisms (Fig. 4). Rear-side X-ray spectra of Cu foil targets irradiated at comparable intensities ($\approx 2-3\times10^{21}$ W/cm^2) produced significant Kα signal at 800 nm and negligible rear-side He-like emission from all target thicknesses. The difference in heating profile is most obvious when comparing the rear-side emission from 1 μm thick foils (Fig. 4 (a)), where only He-like emission was observed at 400 nm. For target thicknesses ≥ 5 μm, both wavelengths produced similar rear-side emission Kα emission lines. For all targets at 800 nm, no He-like or H-like emission was observed from the front surface.

While the absorption fraction from the 800 nm pulses may be expected to exceed the 400 nm due to decrease in laser contrast, increased absorption does not lead to an increase in bulk plasma heating. Bulk heating at 800 nm is reduced due to the existence of an ASE-generated low-density plasma at the target surface [28, 50], in which accelerated electrons propagate before reaching the solid-density target. Strong front sheath fields, which play a key role in controlling the transport dynamics of refluxing electrons and consequently bulk target heating, are also inhibited by this low-density plasma. Sheath fields prevent hot electrons from escaping the target, enabling round trip recirculations within the target until their energy drops below the sheath barrier or the field vanishes [48, 51]. The recirculation time is effectively the sum of the laser pulse duration and the lifetime of the sheath field, which is determined by the energy density of refluxing electrons [52]. The most advantageous conditions for bulk target heating are a combination of lower energy hot electrons and strong sheath fields. At 800 nm, the predicted electron temperatures [53] are $T_{\rm hot} \simeq 3.3$ MeV, while at 400 nm, electron temperatures are $\simeq$1.6 MeV. The lower energy electrons produced by the 400 nm laser are more easily trapped within the target sheath fields, leading to an increase in energy deposition and volumetric heating within the dense plasma [49, 51].

The homogeneous, solid-density, multi-keV plasmas produced in this work were used to examine ionization potential depression (IPD) atomic models. In a plasma, the electrostatic potential surrounding ions can be perturbed by the free charges from neighboring ions and electrons, and as a result the energy required for further ionization can be lowered compared to an equivalent isolated ion. Two popular models of IPD in dense plasmas are Ecker and Kröll (EK) [54] and Stewart and Pyatt (SP) [55]. Previous experiments using the Linear Coherent Light Source and the Orion laser have shown disagreement between which model provides a more accurate description of IPD in dense plasmas [10, 56, 57].

In order to study IPD in HED conditions, the spectral range of the VHS was shifted to 9.5 - 12.5 keV. In Fig. 5, experimental measurements of front-side Cu K-shell emission from 1 μm Cu foils with the 400 nm mode at intensities of 2×10^{21} W/cm^2 (black) is compared with SCRAM simulations using the SP (dashed red) and EK (dash-dotted blue) models. The most apparent differences between the models is in the relative intensity of the Heγ (10.39 keV) to the Heβ (9.87 keV) or Lyβ (10.29 keV) lines; EK appears to overestimate the suppression of the Heγ compared to the Lyβ line at solid densities, whereas SP predicts intensity ratios closer to those observed experimentally. This is in agreement with previous results from Hoarty, et al. [10].

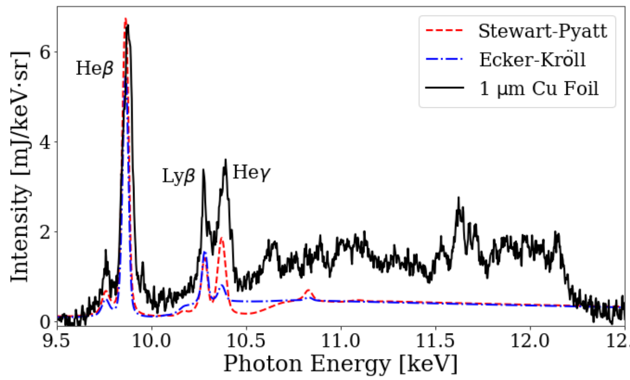

FIG. 5. Front-side emission of 1 μm Cu foils (black) compared to SCRAM spectra using the SP (dashed red) or EK (dash-dotted blue) models.

We have demonstrated the generation of homogeneous HED plasmas using a high-contrast, 400 nm laser at ultra-relativistic intensities. Analysis of K-shell emission from thin copper targets indicates that solid-density plasmas are uniformly heated to multi-keV temperatures at micron depths. SCRAM modeling and collisional PIC simulations were in good agreement with experimental data on the depth and temperatures of these laser-produced plasmas. The significant bulk heating is attributed to the refluxing of MeV electrons produced by the high-contrast, 400 nm mode under the action of target sheath fields. The densities achieved in this work are orders of magnitude higher than the inhomogeneous plasmas commonly generated by multi-ps to ns-scale pulses with densities near $10^{21}-10^{22}$ cm^{-3} [58–60]. The conditions generated at ALEPH are comparable in temperature and ionization states to those obtained using kJ-class picosecond laser systems [15]. Furthermore, the spatial scale and extent of this heating is significantly greater than previously reported [28, 29]. Therefore, this work demonstrates a novel experimental platform method for producing homogeneous, micron-scale HED matter via short-pulse, laser-solid interactions that is crucial for studying HED states of matter.

ACKNOWLEDGMENTS

The authors gratefully acknowledge the assistance of Dr. M. Bailly-Grandvaux and Dr. F. Beg for the use of the spherical crystal imager, the helpful discussions and insight of Dr. B. F. Kraus, and Dr. A. Pukhov for the use of the VLPL code. This work was supported by the U.S. DOE Office of Science, Fusion Energy Sciences and Lawrence Livermore National Lab (Sub-Contract B643845), the Natural Sciences and Engineering Research Council of Canada (Grant No. RGPIN-2021-04373, Hussein), the LaserNetUS initiative at Colorado State University (Contract No. DE-SC-0019076 and DE-SC0021246), and the National Science Foundation (CAREER: National Science Foundation under Grant No. PHY-1753165) and STROBE: A National Science Foundation Science & Technology Center under Grant No. DMR-1548924. JJR and VNS acknowledge support of DoD Vannevar Bush Faculty Fellowship ONR award N000142012842. Sandia National Laboratories is a multimission laboratory managed and operated by National Technology & Engineering Solutions of Sandia, LLC, a wholly owned subsidiary of Honeywell International Inc., for the U.S. Department of Energy's National Nuclear Security Administration under contract DE-NA0003525. KAF was supported by the Laboratory Directed Research and Development program of Los Alamos National Laboratory under project number 20180040DR. This paper describes objective technical results and analysis. Any subjective views or opinions that might be expressed in the paper do not necessarily represent the views of the U.S. Department of Energy or the United States Government.

[1] R. P. Drake, *High-Energy-Density Physics: Foundation of Inertial Fusion and Experimental Astrophysics (Graduate Texts in Physics)* (Springer, 2018).
[2] B. A. Remington, R. P. Drake, and D. D. Ryutov, Rev. Mod. Phys. **78**, 755 (2006).
[3] J. E. Bailey, G. A. Rochau, R. C. Mancini, C. A. Iglesias, J. J. MacFarlane, I. E. Golovkin, C. Blancard, P. Cosse, and G. Faussurier, Phys. Plasmas **16**, 058101 (2009).
[4] J. E. Bailey, T. Nagayama, G. P. Loisel, G. A. Rochau, C. Blancard, J. Colgan, P. Cosse, G. Faussurier, C. J. Fontes, F. Gilleron, I. Golovkin, S. B. Hansen, C. A. Iglesias, D. P. Kilcrease, J. J. MacFarlane, R. C. Mancini, S. N. Nahar, C. Orban, J.-C. Pain, A. K. Pradhan, M. Sherrill, and B. G. Wilson, Nature **517**, 56 (2015).
[5] T. Nagayama, J. E. Bailey, G. P. Loisel, G. S. Dunham, G. A. Rochau, C. Blancard, J. Colgan, P. Cossé, G. Faussurier, C. J. Fontes, F. Gilleron, S. B. Hansen, C. A. Iglesias, I. E. Golovkin, D. P. Kilcrease, J. J. MacFarlane, R. C. Mancini, R. M. More, C. Orban, J.-C. Pain, M. E. Sherrill, and B. G. Wilson, Phys. Rev. Lett. **122**, 235001 (2019).
[6] J. D. Lindl, P. Amendt, R. L. Berger, S. G. Glendinning, S. H. Glenzer, S. W. Haan, R. L. Kauffman, O. L. Landen, and L. J. Suter, Phys. Plasmas **11**, 339 (2004).
[7] M. H. Key, Phys. Plasmas **14**, 055502 (2007).
[8] R. Betti and O. A. Hurricane, Nature Phys **12**, 435 (2016).
[9] S. N. Chen, P. K. Patel, H.-K. Chung, A. J. Kemp, S. Le Pape,

B. R. Maddox, S. C. Wilks, R. B. Stephens, and F. N. Beg, Phys. Plasmas **16**, 062701 (2009).

[10] D. J. Hoarty, P. Allan, S. F. James, C. R. D. Brown, L. M. R. Hobbs, M. P. Hill, J. W. O. Harris, J. Morton, M. G. Brookes, R. Shepherd, J. Dunn, H. Chen, E. Von Marley, P. Beiersdorfer, H. K. Chung, R. W. Lee, G. Brown, and J. Emig, Phys. Rev. Lett. **110**, 265003 (2013).

[11] E. V. Marley, R. Shepherd, P. Beiersdorfer, G. Brown, H. Chen, J. Dunn, M. Foord, H. Scott, R. London, A. B. Steel, D. Hoarty, S. James, C. R. D. Brown, M. Hill, P. Allan, and L. Hobbs, High Energy Density Phys **25**, 15 (2017).

[12] W. J. Gray, M. E. Foord, M. B. Schneider, M. A. Barrios, G. V. Brown, R. F. Heeter, L. C. Jarrott, D. A. Liedahl, E. V. Marley, C. W. Mauche, and K. Widmann, Phys. Plasmas **25**, 062702 (2018).

[13] G. Pérez-Callejo, L. C. Jarrott, D. A. Liedahl, E. V. Marley, G. E. Kemp, R. F. Heeter, J. A. Emig, M. E. Foord, K. Widmann, J. Jaquez, H. Huang, S. J. Rose, J. S. Wark, and M. B. Schneider, Phys. Plasmas **26**, 063302 (2019).

[14] H. Sawada, Y. Sentoku, T. Yabuuchi, U. Zastrau, E. Förster, F. N. Beg, H. Chen, A. J. Kemp, H. S. McLean, P. K. Patel, and Y. Ping, Phys. Rev. Lett. **122**, 155002 (2019).

[15] K. Matsuo, N. Higashi, N. Iwata, S. Sakata, S. Lee, T. Johzaki, H. Sawada, Y. Iwasa, K. F. F. Law, H. Morita, Y. Ochiai, S. Kojima, Y. Abe, M. Hata, T. Sano, H. Nagatomo, A. Sunahara, A. Morace, A. Yogo, M. Nakai, H. Sakagami, T. Ozaki, K. Yamanoi, T. Norimatsu, Y. Nakata, S. Tokita, J. Kawanaka, H. Shiraga, K. Mima, H. Azechi, R. Kodama, Y. Arikawa, Y. Sentoku, and S. Fujioka, Phys. Rev. Lett. **124**, 035001 (2020).

[16] B. F. Kraus, A. Chien, L. Gao, K. W. Hill, M. Bitter, P. C. Efthimion, H. Chen, M. B. Schneider, A. Moreau, R. Hollinger, S. Wang, H. Song, and J. J. Rocca, Review of Scientific Instruments **92**, 033525 (2021).

[17] D. J. Hoarty, S. F. James, C. R. D. Brown, B. M. Williams, T. Guymer, M. Hill, J. Morton, D. Chapman, R. Shepherd, J. Dunn, G. Brown, M. Schneider, P. Beiersdorfer, H. K. Chung, J. W. O. Harris, L. Upcraft, C. C. Smith, and R. W. Lee, J. Phys.: Conf. Ser. **244**, 012002 (2010).

[18] C. R. D. Brown, D. J. Hoarty, S. F. James, D. Swatton, S. J. Hughes, J. W. Morton, T. M. Guymer, M. P. Hill, D. A. Chapman, J. E. Andrew, A. J. Comley, R. Shepherd, J. Dunn, H. Chen, M. Schneider, G. Brown, P. Beiersdorfer, and J. Emig, Phys. Rev. Lett. **106**, 185003 (2011).

[19] B. F. Kraus, L. Gao, K. W. Hill, M. Bitter, P. C. Efthimion, T. A. Gomez, A. Moreau, R. Hollinger, S. Wang, H. Song, J. J. Rocca, and R. C. Mancini, Phys. Rev. Lett. **127**, 205001 (2021).

[20] A. R. Bell, J. R. Davies, and S. M. Guerin, Phys. Rev. E **58**, 2471 (1998).

[21] X. Yang, H. Xu, H. Zhuo, Y. Ma, F. Shao, Y. Yin, and M. Borghesi, Eur. Phys. J. D **68**, 30 (2014).

[22] H. Schmitz and A. P. L. Robinson, Phys. Plasmas **23**, 093104 (2016).

[23] R. G. Evans, E. L. Clark, R. T. Eagleton, A. M. Dunne, R. D. Edwards, W. J. Garbett, T. J. Goldsack, S. James, C. C. Smith, B. R. Thomas, R. Clarke, D. J. Neely, and S. J. Rose, Appl. Phys. Lett. **86**, 191505 (2005).

[24] E. Martinolli, M. Koenig, S. D. Baton, J. J. Santos, F. Amiranoff, D. Batani, E. Perelli-Cippo, F. Scianitti, L. Gremillet, R. Mélizzi, A. Decoster, C. Rousseaux, T. A. Hall, M. H. Key, R. Snavely, A. J. MacKinnon, R. R. Freeman, J. A. King, R. Stephens, D. Neely, and R. J. Clarke, Phys. Rev. E **73**, 046402 (2006).

[25] A. J. Kemp, Y. Sentoku, V. Sotnikov, and S. C. Wilks, Phys. Rev. Lett. **97**, 235001 (2006).

[26] P. M. Nilson, W. Theobald, J. F. Myatt, C. Stoeckl, M. Storm, J. D. Zuegel, R. Betti, D. D. Meyerhofer, and T. C. Sangster, Phys. Rev. E **79**, 016406 (2009).

[27] R. J. Garland, M. Borghesi, and A. P. L. Robinson, Phys. Plasmas **23**, 083116 (2016).

[28] F. Perez, L. Gremillet, M. Koenig, S. D. Baton, P. Audebert, M. Chahid, C. Rousseaux, M. Drouin, E. Lefebvre, T. Vinci, J. Rassuchine, T. Cowan, S. A. Gaillard, K. A. Flippo, and R. Shepherd, Phys. Rev. Lett. **104**, 085001 (2010).

[29] O. N. Rosmej, Z. Samsonova, S. Höfer, D. Kartashov, C. Arda, D. Khaghani, A. Schoenlein, S. Zähter, A. Hoffmann, R. Loetzsch, A. Saevert, I. Uschmann, M. E. Povarnitsyn, N. E. Andreev, L. P. Pugachev, M. C. Kaluza, and C. Spielmann, Phys. Plasmas **25**, 083103 (2018).

[30] R. Hollinger, S. Wang, Y. Wang, A. Moreau, M. G. Capeluto, H. Song, A. Rockwood, E. Bayarsaikhan, V. Kaymak, A. Pukhov, V. N. Shlyaptsev, and J. J. Rocca, Nat. Photonics **14**, 607 (2020).

[31] K. Yasuike, M. H. Key, S. P. Hatchett, R. A. Snavely, and K. B. Wharton, Rev. Sci. Instrum. **72**, 1236 (2001).

[32] G. Gregori, S. B. Hansen, R. Clarke, R. Heathcote, M. H. Key, J. King, R. I. Klein, N. Izumi, A. J. Mackinnon, S. J. Moon, H.-S. Park, J. Pasley, N. Patel, P. K. Patel, B. A. Remington, D. D. Ryutov, R. Shepherd, R. A. Snavely, S. C. Wilks, B. B. Zhang, and S. H. Glenzer, Contrib. Plasma Phys. **45**, 284 (2005).

[33] W. Theobald, K. Akli, R. Clarke, J. A. Delettrez, R. R. Freeman, S. Glenzer, J. Green, G. Gregori, R. Heathcote, N. Izumi, J. A. King, J. A. Koch, J. Kuba, K. Lancaster, A. J. MacKinnon, M. Key, C. Mileham, J. Myatt, D. Neely, P. A. Norreys, H.-S. Park, J. Pasley, P. Patel, S. P. Regan, H. Sawada, R. Shepherd, R. Snavely, R. B. Stephens, C. Stoeckl, M. Storm, B. Zhang, and T. C. Sangster, Phys. Plasmas **13**, 043102 (2006).

[34] K. U. Akli, M. H. Key, H. K. Chung, S. B. Hansen, R. R. Freeman, M. H. Chen, G. Gregori, S. Hatchett, D. Hey, N. Izumi, J. King, J. Kuba, P. Norreys, A. J. Mackinnon, C. D. Murphy, R. Snavely, R. B. Stephens, C. Stoeckel, W. Theobald, and B. Zhang, Phys. Plasmas **14**, 023102 (2007).

[35] C. M. Huntington, C. C. Kuranz, G. Malamud, R. P. Drake, H.-S. Park, and B. R. Maddox, Rev. Sci. Instrum. **83**, 10E114 (2012).

[36] P. Palmeri, G. Boutoux, D. Batani, and P. Quinet, Phys. Rev. E **92**, 033108 (2015).

[37] I. Y. Skobelev, S. N. Ryazantsev, D. D. Arich, P. S. Bratchenko, A. Y. Faenov, T. A. Pikuz, P. Durey, L. Doehl, D. Farley, C. D. Baird, K. L. Lancaster, C. D. Murphy, N. Booth, C. Spindloe, P. McKenna, S. B. Hansen, J. Colgan, R. Kodama, N. Woolsey, and S. A. Pikuz, Photon. Res., PRJ **6**, 234 (2018).

[38] F. N. Beg, A. R. Bell, A. E. Dangor, C. N. Danson, A. P. Fews, M. E. Glinsky, B. A. Hammel, P. Lee, P. A. Norreys, and M. Tatarakis, Phys. Plasmas **4**, 447 (1997).

[39] C. Reich, I. Uschmann, F. Ewald, S. Düsterer, A. Lübcke, H. Schwoerer, R. Sauerbrey, E. Förster, and P. Gibbon, Phys. Rev. E **68**, 056408 (2003).

[40] Y. Wang, S. Wang, A. Rockwood, B. M. Luther, R. Hollinger, A. Curtis, C. Calvi, C. S. Menoni, and J. J. Rocca, Opt. Lett., OL **42**, 3828 (2017).

[41] See supplemental material at [url to be inserted by publisher] for further discussion, which includes ref [61].

[42] S. B. Hansen, J. Bauche, C. Bauche-Arnoult, and M. F. Gu, High Energy Density Phys Radiative Properties of Hot Dense Matter, **3**, 109 (2007).

[43] A. Pukhov, J. Plasma Phys. **61**, 425 (1999).

[44] A. H. Gabriel, Monthly Notices of the Royal Astronomical Society **160**, 99 (1972).

[45] O. N. Rosmej and F. B. Rosmej, Nucl Instrum Methods Phys Res B The Physics of Highly Charged Ions, **98**, 37 (1995).
[46] S. H. Glenzer, C. A. Back, K. G. Estabrook, B. J. MacGowan, D. S. Montgomery, R. K. Kirkwood, J. D. Moody, D. H. Munro, and G. F. Stone, Phys. Rev. E **55**, 927 (1997).
[47] J. P. Apruzese, J. Davis, K. G. Whitney, J. W. Thornhill, P. C. Kepple, R. W. Clark, C. Deeney, C. A. Coverdale, and T. W. L. Sanford, Phys. Plasmas **9**, 2411 (2002).
[48] J. Myatt, W. Theobald, J. A. Delettrez, C. Stoeckl, M. Storm, T. C. Sangster, A. V. Maximov, and R. W. Short, Phys Plasmas **14**, 056301 (2007).
[49] L. G. Huang, T. Kluge, and T. E. Cowan, Phys. Plasmas **23**, 063112 (2016).
[50] S. D. Baton, M. Koenig, J. Fuchs, A. Benuzzi-Mounaix, P. Guillou, B. Loupias, T. Vinci, L. Gremillet, C. Rousseaux, M. Drouin, E. Lefebvre, F. Dorchies, C. Fourment, J. J. Santos, D. Batani, A. Morace, R. Redaelli, M. Nakatsutsumi, R. Kodama, A. Nishida, N. Ozaki, T. Norimatsu, Y. Aglitskiy, S. Atzeni, and A. Schiavi, Physics of Plasmas **15**, 042706 (2008).
[51] L. G. Huang, M. Molodtsova, A. Ferrari, A. L. Garcia, T. Toncian, and T. E. Cowan, Phys. Plasmas **29**, 023102 (2022).
[52] P. Mora, Physical Review Letters **90**, 185002 (2003).
[53] T. Kluge, T. Cowan, A. Debus, U. Schramm, K. Zeil, and M. Bussmann, Phys. Rev. Lett. **107**, 205003 (2011).
[54] G. Ecker and W. Kröll, Phys. Fluids **6**, 62 (1963).
[55] J. C. Stewart and K. D. Pyatt, Jr., Astrophys. J. **144**, 1203 (1966).
[56] O. Ciricosta, S. M. Vinko, H.-K. Chung, B.-I. Cho, C. R. D. Brown, T. Burian, J. Chalupský, K. Engelhorn, R. W. Falcone, C. Graves, V. Hájková, A. Higginbotham, L. Juha, J. Krzywinski, H. J. Lee, M. Messerschmidt, C. D. Murphy, Y. Ping, D. S. Rackstraw, A. Scherz, W. Schlotter, S. Toleikis, J. J. Turner, L. Vysin, T. Wang, B. Wu, U. Zastrau, D. Zhu, R. W. Lee, P. Heimann, B. Nagler, and J. S. Wark, Phys. Rev. Lett. **109**, 065002 (2012).
[57] O. Ciricosta, S. M. Vinko, B. Barbrel, D. S. Rackstraw, T. R. Preston, T. Burian, J. Chalupský, B. I. Cho, H.-K. Chung, G. L. Dakovski, K. Engelhorn, V. Hájková, P. Heimann, M. Holmes, L. Juha, J. Krzywinski, R. W. Lee, S. Toleikis, J. J. Turner, U. Zastrau, and J. S. Wark, Nat. Commun. **7**, 11713 (2016).
[58] J. Filevich, J. J. Rocca, M. C. Marconi, R. F. Smith, J. Dunn, R. Keenan, J. R. Hunter, S. J. Moon, J. Nilsen, A. Ng, and V. N. Shlyaptsev, Appl. Opt., AO **43**, 3938 (2004).
[59] R. F. Heeter, S. B. Hansen, K. B. Fournier, M. E. Foord, D. H. Froula, A. J. Mackinnon, M. J. May, M. B. Schneider, and B. K. F. Young, Phys. Rev. Lett. **99**, 195001 (2007).
[60] M. J. May, M. B. Schneider, S. B. Hansen, H. K. Chung, D. E. Hinkel, H. A. Baldis, and C. Constantin, High Energy Density Physics **4**, 78 (2008).
[61] R. Hollinger, (to be published).